Substrate-specific regulation of the mTORC1 pathway by G protein-coupled receptors

Samuel J. Atkinson[1], Florentina Negoita[2], William Vincent Ritchie[1], Kyle Thompson[1], Kei Sakamoto[2], Dawn Thompson[1], James N. Hislop[1]*, and Riko Hatakeyama[1]*

[1]Institute of Medical Sciences, School of Medicine, Medical Sciences & Nutrition, University of Aberdeen

[2]Novo Nordisk Foundation Center for Basic Metabolic Research, University of Copenhagen

*Corresponding authors;

riko.hatakeyama@abdn.ac.uk

ORCID 0000-0002-3065-6639

Institute of Medical Sciences, University of Aberdeen, Foresterhill, Aberdeen AB25 2ZD, UK

james.hislop@abdn.ac.uk

ORCID 0000-0002-4829-7531

Institute of Medical Sciences, University of Aberdeen, Foresterhill, Aberdeen AB25 2ZD, UK

Running title

Substrate-specific GPCR-mTORC1 signaling

Keywords

mammalian/mechanistic Target of Rapamycin Complex 1 (mTORC1); G protein-coupled receptor (GPCR); muscarinic acetylcholine receptor M5 (M5R)

Abbreviations

mTORC1: mammalian/mechanistic Target of Rapamycin Complex 1

GPCR: G protein-coupled receptor

M5R: muscarinic acetylcholine receptor M5

FPR2: formyl peptide receptor 2

β2AR: beta-2 adrenergic receptor

DREADD: designer receptor exclusively activated by designer drugs

CNO: Clozapine N-oxide

PKC: protein kinase C

Abstract

The mammalian/mechanistic Target of Rapamycin Complex 1 (mTORC1) orchestrates cell growth and metabolism in response to diverse external cues. mTORC1 has a myriad of phosphorylation substrates, each playing important physiological roles. Emerging evidence suggests that mTORC1 can respond to upstream signals in a nuanced manner, enabling differential regulation of individual substrates and downstream biological processes. However, the nature of signals that determine the signaling selectivity of mTORC1 remains incompletely understood. Here, we studied mTORC1 regulation by G protein-coupled receptors (GPCRs). We found that phosphorylation of the Transcription Factor EB (TFEB), a non-canonical mTORC1 substrate that controls lysosome biogenesis, responds to GPCRs differently, compared to canonical mTORC1 substrates controlling protein synthesis such as S6K1 and 4EBP1. In particular, the muscarinic acetylcholine receptor M5 (M5R) promoted phosphorylation of S6K1 and 4EBP1, while triggering TFEB dephosphorylation. Consequently, M5R stimulated protein synthesis without inhibiting lysosome biogenesis. The regulations of an anabolic process and a catabolic process, albeit both governed by mTORC1, are thus decoupled downstream of M5R. This study highlights the importance of reassessing the effects of GPCRs on mTORC1 by concurrently monitoring individual substrates, a critical consideration to be made when evaluating GPCR ligands as therapeutic agents targeting the mTORC1 pathway.

48 # Introduction

49 Cells adapt to the changing environment by fine-tuning various biological processes. At the core of
50 the cellular adaptation mechanism is the mammalian/mechanistic Target of Rapamycin Complex 1
51 (mTORC1), a master regulator of cell growth and metabolism (1)(2). mTORC1 is a serine/threonine
52 kinase that gets activated by pro-growth signals such as nutrients (e.g., amino acids) and growth
53 factors (e.g., insulin). mTORC1, in turn, activates pro-growth cellular processes such as anabolic
54 reactions (e.g. protein synthesis) while repressing catabolic reactions (e.g. protein degradation via
55 autophagy), through phosphorylating its substrate proteins. mTORC1 activation by amino acids and
56 by insulin/growth factors is mediated by Rag and Rheb small GTPases, respectively. mTORC1 plays a
57 pivotal role in cellular/organismal homeostasis in humans and is implicated in a range of conditions,
58 including cancer, diabetes, neurodegeneration, and aging. Developing effective therapeutic strategies
59 for these diseases requires a deeper mechanistic understanding of mTORC1 regulation.

60 An emerging theme in the mTORC1 research field is mTORC1's differential signaling to individual
61 substrates. Depending on upstream stimuli, the phosphorylation patterns of several "non-canonical"
62 mTORC1 substrates including the transcription factor EB (TFEB), a regulator of lysosome biogenesis,
63 responds differently to that of canonical mTORC1 substrates such as the ribosomal protein S6 kinase
64 1 (S6K1) and the eukaryotic translation initiation factor 4E-binding protein 1 (4EBP1), regulators of
65 global protein synthesis (3)(4)(5). Unlike phosphorylation of canonical substrates that requires
66 activation of both Rag and Rheb small GTPases, TFEB phosphorylation is thought to only respond to
67 Rag GTPases.

68 Two models have been proposed to explain the distinct behavior of TFEB, which are not mutually
69 exclusive. One model attributes the difference to the unique substrate recruitment mechanism, in
70 which Rag GTPases physically interact with TFEB (but not S6K1 or 4EBP1) and present it to mTORC1
71 (3)(6). Another model assigns these substrates to spatially distinct mTORC1 pools; the cytosolic
72 mTORC1 pool phosphorylates S6K1 and 4EBP1, while the lysosomal mTORC1 pool phosphorylates
73 TFEB (5). In either case, a comprehensive view is missing on how various external cues, that are
74 typically sensed by cell-surface receptors, differentially feed into individual mTORC1 substrates.

75 G protein-coupled receptors (GPCRs) constitute the largest cell-surface receptor family, being
76 encoded by more than 800 genes in the human genome (7)(8). GPCRs sense diverse signals ranging
77 from chemicals such as growth factors and odorants to physical parameters such as light.
78 Characterizing any GPCR-mTORC1 signaling therefore has wide-reaching implications for cellular
79 adaptation mechanisms operating in diverse contexts across the human body. Moreover, GPCRs are
80 highly druggable proteins, as more than 30% of FDA-approved drugs target GPCRs (9). To harness the
81 therapeutic potential of these drugs and enable their safe and effective repurposing across diverse
82 diseases, it is essential to elucidate how G protein–coupled receptors (GPCRs) transmit signal to
83 downstream pathways such as the mTORC1 pathway.

84 For many years GPCR signaling was thought to occur exclusively via activation of heterotrimeric G-
85 proteins, with distinct Gα subtypes triggering distinct downstream events. G_q stimulates
86 phospholipase C; G_s and G_i stimulates and inhibits, respectively, cyclic AMP production; $G_{12/13}$
87 activates Rho small GTPases (10)(11). This original paradigm has since been challenged, with the
88 identification of G protein-independent signaling cascades, often proposed to be mediated by β-
89 arrestin proteins (12). More recently, the GPCR field has undergone a further paradigm shift. Both G-
90 protein dependent and -independent signaling can occur from intracellular compartments,
91 particularly endosomes, previously thought to be refractory for signaling (13). However, the role of
92 intracellular signaling remains poorly understood, particularly in the context of mTORC1 regulation.

93 Substantial efforts have been made to elucidate how GPCRs modulate mTORC1 signaling (reviewed
94 in (14)), with some GPCRs shown to activate, while others inhibit, mTORC1. A largely overlooked
95 aspect, however, is the substrate specificity of GPCR-mTORC1 signaling, as most prior studies
96 monitored phosphorylation of only canonical mTORC1 substrates such as S6K1 and/or 4EBP1. In this
97 study, we examined in parallel the response of S6K1, 4EBP1, and the non-canonical mTORC1
98 substrate TFEB to GPCR stimulation. We found that TFEB responds to GPCR stimulation differently to
99 S6K1 and 4EBP1, allowing simultaneous operation of protein synthesis and lysosome biogenesis. Our
100 findings reveal substrate/downstream specificity as a novel layer of the GPCR-mTORC1 signaling.

101

102 Results

103 Development of M5R-DREADD cell line

104 We examined how phosphorylation of various mTORC1 substrates —S6K1, 4EBP1, and TFEB—
105 responds to GPCR stimulation. As G_q has been previously implicated in mTORC1 signaling (14), we
106 investigated a G_q-coupled GPCR with the muscarinic acetylcholine receptor M5 (M5R) as a model.

107 Acetylcholine, the endogenous ligand of M5R, stimulates nicotinic and muscarinic receptor subtypes,
108 a number of which are endogenously expressed in HEK293 cells (15) (Figure 1A left). To specifically
109 observe the effects of M5R activation, we developed a system to selectively stimulate M5R. We took
110 advantage of the previously described mutations that make muscarinic receptors into 'designer
111 receptor exclusively activated by designer drugs (DREADD)' receptors, which are uniquely activated
112 by the synthetic ligand clozapine N-oxide (CNO) (Figure 1A right) (16).

113 We generated a HEK293 cell line stably expressing M5R-DREADD. The M5R-DREADD cells responded
114 to CNO in a dose-dependent manner as expected, triggering phosphorylation of its downstream MAP
115 kinase ERK1/2 (Figure 1B and 1C, showing the activation kinetics and concentration-response curve,
116 respectively). CNO robustly enhanced the metabolic activity (reducing power) of serum-starved M5R-
117 DREADD cells (Figure 1D), suggesting the positive role of M5R in cell growth and/or proliferation. Our
118 data established the M5R-DREADD cell line as a useful model to investigate growth/proliferation
119 signaling, including the mTORC1 pathway.

120

121 M5R regulates mTORC1 in a substrate-specific manner

122 We examined phosphorylation of canonical mTORC1 substrates, S6K1 and 4EBP1, that promote
123 global protein synthesis. We serum-starved M5R-DREADD cells to bring the mTORC1 activity down to
124 a basal level before stimulation with CNO. CNO treatment triggered phosphorylation of S6K1, as
125 probed by the phospho-specific antibody (Figure 2A and 2B, panel 1, for a short and long time-course,
126 respectively). This effect of CNO was specifically through M5R stimulation, because it was not seen in
127 the parental wild-type HEK293 line not expressing M5R-DREADD (Figure 2C). Phosphorylation of
128 S6K1 coincided with that of 4EBP1, which was detected as a stereotypical shift in banding pattern to
129 that of higher molecular weight species (Figure 2A and 2B, panel 3).

130 We then examined the lysosome biogenesis regulator TFEB, as its phosphorylation by mTORC1 is
131 regulated in a non-canonical, Rheb-independent manner. Strikingly, phosphorylation of TFEB, as
132 probed by the phospho-specific antibody, was rather downregulated by CNO treatment after 16
133 minutes (Figure 2A and 2B, panel 4). These results suggest that M5R activates mTORC1 towards S6K1
134 and 4EBP1, while inhibiting it towards TFEB (Figure 2D).

135 We noticed the slow kinetics of mTORC1 substrate phosphorylation by M5R, which did not peak until
136 32 minutes in the case of S6K1 (Figure 2A and 2B, panel 1). This was in stark contrast to the kinetics
137 of ERK1/2 phosphorylation that peaked at, or potentially even before, 4 minutes of CNO treatment
138 (Figure 2A, panel 6). This observation raises the intriguing possibility that mTORC1 is activated only
139 after M5R is internalized (see later). M5R appears to transmit qualitatively different signals over time,
140 an early signal via ERK1/2 and a late signal via mTORC1.

141

142 **M5R stimulates protein synthesis**

143 Having observed the opposite effects of M5R activation on phosphorylation of canonical substrates
144 (S6K1 and 4EBP1) and that of TFEB, we then examined further downstream cellular processes.
145 Phosphorylation of S6K1 and 4EBP1 by mTORC1 promotes global protein synthesis (1)(2). S6K1 exerts
146 this effect partly through phosphorylation of the ribosomal protein S6. As expected, CNO robustly
147 triggered S6 phosphorylation in M5R-DREADD cells (Figure 3A).

148 *De novo* protein synthesis can be monitored by the established puromycin incorporation assay (17).
149 As shown in Figure 3B, serum starvation caused decreased incorporation of puromycin, suggestive of
150 slowed protein synthesis. Subsequent M5R stimulation by CNO triggered increased puromycin
151 incorporation. These results revealed the positive effect of M5R signaling on cellular protein
152 synthesis activity, consistent with increased phosphorylation of S6K1 and 4EBP1.

153

154 **M5R does not inhibit lysosome biogenesis**

155 M5R stimulation caused dephosphorylation of TFEB (Figure 2A and 2B). TFEB dephosphorylation
156 upon amino acid starvation triggers its nuclear translocation, and through activating a transcriptional
157 program, promotes lysosome biogenesis (18). We examined these downstream events upon M5R
158 stimulation.

159 As expected, CNO treatment in serum-starved M5R-DREADD cells triggered nuclear translocation of
160 TFEB-GFP, similar to amino acid-starved cells (Figure 4A). We confirmed this result by cellular
161 fractionation of cytosol and nuclei. In both serum-fed and -starved cells, more TFEB was detected in
162 the nuclear fraction in CNO-treated samples (Figure 4B, panel 1). The mTOR inhibitor Torin1 similarly
163 caused nuclear translocation of TFEB, as previously reported (18).

164 We then quantified lysosomes using a fluorescent lysosome-staining dye (Lysotracker). As shown in
165 Figure 4C, serum starvation increased the intensity of Lysotracker signal and the number of
166 Lysotracker-positive lysosomes, suggestive of enhanced lysosome biogenesis. This trend was not
167 reversed by subsequent M5R stimulation by CNO, in contrast to the recovery in protein synthesis
168 (Figure 3B). The fact that we did not observe a further increase of lysosomes suggests that M5R-
169 driven dephosphorylation of TFEB is not sufficient to increase lysosome biogenesis in our
170 experimental setting.

171 Taken together, M5R activation promoted protein synthesis without suppressing lysosome biogenesis.
172 This observation was consistent with the differential effect of M5R stimulation on phosphorylation of
173 S6K1 and 4EBP1, and that of TFEB (Figure 2D). We conclude that M5R regulates mTORC1 in a
174 substrate/downstream-specific manner.

175

176 **Mechanistic insights into the M5R-mTORC1 signaling**

177 We next addressed the mechanism of M5R-mTORC1 signaling. Because M5R activates the
178 phospholipase C-protein kinase C (PKC) pathway downstream of G_q (Figure 5A, left) (10)(11), we
179 examined the effect of the PKC inhibitor GF109203x. As shown in Figure 5B, CNO-triggered
180 phosphorylation of S6K1 and 4EBP1 in M5R-DREADD cells was blocked by GF109203x (lanes 4 and 5,
181 panels 1 and 3), suggesting that mTORC1 activation towards S6K1 and 4EBP1 requires PKC activity.

182 We were unable to assess the role of PKC in the M5R-triggered dephosphorylation of TFEB, because
183 TFEB did not respond to CNO in this experiment (lanes 3 and 4, panel 4). This was due to an
184 unexpected effect of DMSO, which was used as the solvent of GF109203x as well as the mock
185 control— we noticed that the DMSO treatment alone causes severe dephosphorylation of TFEB
186 (Figure 5C). As an additional note, the effects of CNO and DMSO differed in that only the former
187 caused a downshift of the total TFEB band (panel 2), suggesting that M5R also regulates
188 posttranslational modification(s) of TFEB other than its Serine 122 phosphorylation.

189 As GPCRs signal from both the plasma membrane and endosomes (13), we asked where M5R signals
190 to mTORC1. The remarkably slow kinetics of mTORC1's response to CNO led us to hypothesize that
191 M5R only signals to mTORC1 after being internalized. We addressed this possibility using the
192 dynamin inhibitor Dyngo-4a that blocks endocytosis (19). As shown in Figure 5D (lanes 4 and 5,
193 panels 1 and 3), Dyngo-4a significantly blocked phosphorylation of S6K1 and 4EBP1 triggered by M5R.
194 This observation favours the post-internalization signaling model, as recently proposed by others (20).
195 Our results did not inform the location where M5R signals to the mTORC1-TFEB axis, because of the
196 issue of DMSO (Figure 5C), in which Dyngo-4a was dissolved.

197 mTORC1 is activated by the actions of Rag and Rheb small GTPases, which mediate amino acid and
198 insulin/growth factor signals, respectively (Figure 5A, right). Notably, M5R failed to stimulate S6K1
199 and 4EBP1 phosphorylation in amino acid-starved cells (Figure 5E, lanes 2 and 6, panels 1 and 3;
200 compare with serum-starved cells in lanes 3 and 7). This was not due to the failure of M5R activation,
201 because ERK1/2 phosphorylation was similarly triggered by CNO in serum- and amino acid-starved
202 cells (lanes 6 and 7, panel 6). Hence, M5R seems to activate the Rheb branch but not the Rag branch,
203 the latter of which requires an amino acid signal.

204 Growth factors, including insulin, activate Rheb via the mTORC2-Akt cascade (Figure 5A, right). M5R
205 does not activate this canonical upstream pathway, because CNO did not promote phosphorylation
206 of Akt and TSC2, an Akt substrate (Figure 5F). These phosphorylation events were rather
207 downregulated by CNO, which could be due to the known negative feedback regulation through
208 S6K1 (Figure 5A, right).

209 Altogether, the most straightforward interpretation of our data is that M5R activates the mTORC1-
210 S6K1/4EBP1 axis through the G_q-PKC pathway after being internalized. This signal most likely
211 impinges on Rheb, through unknown mechanisms independent from the canonical mTORC2-Akt-TSC
212 pathway. How M5R inhibits the mTORC1-TFEB axis is less clear.

213

214 **mTORC1 regulation by FPR2 and β2AR**

215 To gain broader insight, we asked whether substrate-specific regulation of mTORC1 is unique to
216 M5R/G_q-coupled GPCRs. We examined the G_i-coupled formyl peptide receptor 2 (FPR2). FPR2-
217 expressing HEK293 cells previously generated (21) were serum starved and treated with the peptide
218 ligand WKYMVm, a potent FPR2 agonist. As shown in Figure 6A, WKYMVm triggered phosphorylation

219 of S6K1 and 4EBP1 in 16 minutes (panels 1 and 3), though not affecting the cellular metabolic activity
220 (Figure 6B). S6 phosphorylation was promoted as expected (Figure 6C). Unlike M5R, FPR2 did not
221 strongly inhibit TFEB phosphorylation (Figure 6A, panel 4). Lysosome biogenesis was unaffected
222 (Figure 6D).

223 We then examined G_S-coupled GPCRs. We treated wild-type HEK293 cells, which endogenously
224 express the G_S-coupled beta-2 and -1 adrenergic receptors (β2AR and β1AR), with their ligand
225 isoprenaline. Isoprenaline triggered phosphorylation of S6K1 in 64 minutes (Figure 6E, panel 1), but
226 did not cause a clear band shift of 4EBP1 (panel 3). Isoprenaline did not affect cellular metabolic
227 activity (Figure 6F), despite increased S6 phosphorylation (Figure 6G). TFEB phosphorylation was not
228 inhibited (Figure 6E, panel 4), with lysosome biogenesis unaffected (Figure 6H).

229 To summarize, M5R, FPR2, and β2AR/β1AR all activated mTORC1 towards S6K1. M5R and FPR2 also
230 activated the mTORC1-4EBP1 branch. However, M5R inhibited mTORC1 towards TFEB, uniquely
231 among the three GPCRs. Hence, different GPCRs regulate mTORC1 with varied substrate specificities.

232

233 # Discussion

234 This study uncovered the substrate/downstream-specific mode of mTORC1 regulation by GPCRs,
235 revealing an additional layer of complexity to this signaling axis. Notably, the response of TFEB was
236 very different (even opposite for M5R) from that of canonical mTORC1 substrates, S6K1 and 4EBP1. A
237 lesson to be drawn from this is that we need to monitor multiple mTORC1 substrates including TFEB
238 when assessing the effects of GPCRs. This perspective has been largely overlooked in previous
239 studies, which have predominantly focused on canonical mTORC1 targets (14).

240 Mechanistically, the unique response of TFEB upon GPCR stimulation can be partly explained if
241 GPCRs signal to mTORC1 through the Rheb branch, which TFEB is uniquely unresponsive to. This
242 interpretation aligns with our observation that M5R stimulation overrides FBS starvation but not
243 amino acid starvation (Figure 5E). It is indeed known that the MEK-ERK1/2 cascade, which acts
244 downstream of many GPCRs including the ones examined here, activates Rheb by inhibiting its
245 negative regulator TSC complex (22). Another factor could be the subcellular location of
246 phosphorylation events. Given that TFEB is phosphorylated at lysosomes rather than the cytoplasm
247 as proposed for S6K1 and 4EBP1 (5), GPCRs may exert substrate-specific effects by modulating
248 mTORC1 localization or location-specific activities. The involvement of phosphatases antagonizing
249 mTORC1 should also be considered, which could be different for each mTORC1 substrate (4).

250 The non-canonical response of TFEB observed in this and other studies indicates the regulatory
251 decoupling of a catabolic process (lysosome biogenesis) from an anabolic process (protein synthesis),
252 even though both are governed by mTORC1. A similar decoupling is observed in the budding yeast
253 model, in which protein synthesis and autophagy are regulated by spatially distinct TORC1 pools (23).
254 This may look counterintuitive from the traditional view in the TORC1 field that activation of
255 anabolism or catabolism should coincide with inhibition of the other. Such coupling would make
256 sense in the context of nutrient response, where cells adapt their bulk mass to nutrient availability.
257 However, the situation is different when cells respond to other stimuli such as growth factors or
258 stresses. Cells would need to change themselves qualitatively by remodelling the proteome, not
259 necessarily changing their total mass. For that, they would need to synthesize proteins that are
260 needed in the new environment, and simultaneously degrade proteins not needed anymore. The
261 latter catabolic process and subsequent recycling of resources (e.g., amino acids) fuel the former

anabolic processes. In such a situation, it would be beneficial to activate both anabolism and catabolism by decoupling their regulations.

There is another potential benefit of metabolic decoupling in light of cell proliferation. M5R robustly stimulated cellular metabolic activity (Figure 1D). Under this condition where cells actively proliferate, it would be beneficial to keep TFEB dephosphorylated and generate lysosomes needed for daughter cells. TFEB dephosphorylation was indeed not observed upon FPR2 or β2AR/β1AR activation, where cellular metabolic activity was unaffected (Figure 6).

The supreme druggability of GPCRs, and their tissue/context-specific expression patterns, make GPCR ligands attractive therapeutic tools to manipulate mTORC1 pathway to treat cancer, diabetes, neurodegeneration, and aging. The substrate/downstream specificity revealed in this study further enhances the potential of GPCR ligands, as it theoretically enables selective manipulation of the desired downstream functions of mTORC1, which should be more effective and safer than pan-mTORC1 manipulation. This transformative potential warrants a comprehensive investigation of the mTORC1 substrate specificity for a wider range of GPCRs.

Materials and methods

Antibodies and reagents

All antibodies were purchased from Cell Signaling Technologies except anti-GAPDH (Proteintech 60004-1-Ig). Anti-S6K (2708), anti-phospho-S6K Thr389 (9205), anti-4EBP1 (9644), anti-TFEB (4240), anti-phospho-TFEB Ser122 (87932), anti-S6 (2217), anti-phospho-S6 Ser240/Ser244 (5364) anti-phospho-p44/42 MAPK (Erk1/2) Thr202/Tyr204 (4370), anti-anti-Vinculin (13901), anti-Lamin A/C (4777), anti-Akt (4691), anti-phospho-Akt Ser473 (4060), anti-TSC2 (4308), and anti-phospho-TSC2 Thr1462 (3617) were used at 1:1000. Anti-GAPDH was used at 1:30,000. Unless otherwise stated, common reagents were purchased from Thermo Fisher Scientific.

Cell culture

All cell lines (HEK293 and derivatives) were cultured in DMEM high glucose (Merck D5671) supplemented with 1 mM sodium pyruvate (Thermo Fisher Scientific 11360-039), 1% glutamine (Merck G7513) and 10% FBS (Biosera 10011500) at 37°C in an atmosphere of 5% CO_2. Cell lines were regularly tested for the presence of mycoplasma contamination. FPR2 stably expressing cells were previously generated as described in (21). DMEM without amino acids (VWR USBID9800-13) was supplemented with glucose to match DMEM high glucose above, 1 mM sodium pyruvate and 10% dialysed FBS (lacking amino acids). For dialysing FBS, the same FBS batch used for all experiments was dialysed against PBS twice overnight at 4°C using a 3500 Da cutoff Snakeskin™ dialysis membrane (Thermo Fisher Scientific 88242).

Muscarinic Acetylcholine Receptor M5 DREADD stable cell line

HEK293 cells were from the ATCC. The M5 DREADD receptor was generated based on the M3R DREADD (24). Briefly, M5R cDNA was obtained from cDNA.org and subcloned into the Flag pcDNA3.1+ zeo (21). Site-directed mutagenesis (QuickChange, Agilent) was then used to introduce the mutations in the 3rd and 5th transmembrane domain (Y111C and A201G) to confer sensitivity to CNO. Stables were generated by selection with zeocin and identified by anti-Flag immunofluorescence determined by microscopy.

GPCR stimulation

All cell lines were washed with PBS and then starved of amino acids or FBS for 2 hours before treatment with the GPCR antagonists at 1 µM: CNO (Tocris/bio-techne 6329), Isoprenaline (Sigma/Merck I6504) or WKYMVm (Tocris/BioTechne 1800) in M5R-DREADD, wild-type or FPR2-expressing HEK293 cells, respectively, for the indicated timepoints. For inhibitor experiments: 10 µM Dyngo®-4a (Abcam ab120689) or 5 µM PKC inhibitor GF109203x (Sigma/Merck B6292) was added to the culture media 30 minutes or 1.5 hours, respectively, before GPCR stimulation. 100 nM Torin1 was applied for 32 minutes.

Global translation assay

Cells were stimulated as above, and puromycin (Thermo Fisher Scientific 227420500) was added 15 minutes before lysis at 5 µg/ml as per the SUNSET assay protocol (17).

Cellular fractionation

Cellular fractionation was performed with the NE-PER™ Nuclear and Cytoplasmic Extraction Reagents kit (Thermo Fisher Scientific, 78835). The cells were seeded in 6-well plates at a cell density of $4x10^5$ cells/well. The next day they were treated as specified in the figure legends. After treatment, the

318 cells were washed once with PBS (Substrate and Sterile Centre, University of Copenhagen). The
319 washed cells were lysed with the cytosolic extraction reagents I and II (CERI and CERII) provided in
320 the kit, to induce disruption of the cell membranes and the release of cytosolic proteins. After being
321 scrapped in cold CERI buffer containing protease and phosphatase inhibitors (500 µM
322 phenylmethylsulfonyl fluoride (PMSF [Sigma, P7626]), 1 mM benzamidine hydrochloride [Sigma,
323 199001], 1 µg/ml leupeptin [Sigma, L2884], 1 µg/ml pepstatin A [Sigma, P5318], 1 µM microcystin-LR
324 [Enzo Life Sciences, ALX-350-012], 1 mM sodium orthovanadate [Sigma, S6508]), the cells in CERI
325 buffer were dispersed by brief vortexing, incubated on ice for 10 min and then, mixed with CERII
326 buffer and further incubated on ice for 1 min. The separation of cytosolic proteins from the nuclear
327 pellet was performed by centrifugation at 16,000 x g for 5 min at 4°C. The supernatant containing the
328 cytosolic protein fraction was collected in a new tube and denatured at 100°C for 5 min in Laemmli
329 sample buffer (50 mM Tris, pH 6.8, 2% sodium dodecyl sulfate [Sigma, 74255], 0.5 mM EDTA (Sigma,
330 E5134), 10% glycerol [Sigma, G5516], 0.01% bromophenol blue [Sigma, 114391]). The pellet
331 containing the nuclei was washed three times with cold PBS. Nuclear protein fractions were obtained
332 by extraction from the nuclear pellet with Laemmli sample buffer at 100°C for 7 min. The denatured
333 cytosolic and nuclear protein fractions were stored at -20°C until Western blot analysis.

334 **Western blotting**

335 Cells were washed with PBS before being lysed directly in high SDS lysis buffer (3% SDS, 60 mM
336 sucrose, 65 mM Tris-HCl pH 6.8), denatured at 95°C for 5 minutes, homogenised by sonication and
337 cleared by centrifugation at 18,000 x g for 30 minutes. Lysates were quantified by a linearised
338 Bradford assay (Abcam ab119216) using a 595 nm/450 nm ratio.

339 25 µg of proteins were separated in SDS-PAGE gels before being transferred to nitrocellulose
340 membranes (VWR 10600002). After ponceau staining, membranes were blocked with 5% milk/TBST
341 (for anti-TFEB, phospho-TFEB, GAPDH, and phospho-MAPK antibodies), 3% milk/TBST (for anti-
342 Vinculin, Lamin A/C, Akt, phospho-Akt, TSC2, and phospho-TSC2 antibodies) or 5% BSA/TBST (for
343 anti-S6K, phospho-S6K, and 4EBP1 antibodies) and probed with antibodies overnight at 4°C in 5%
344 BSA/TBST (for anti-S6K, phospho-S6K, 4EBP1, TFEB, phospho-TFEB, and phospho-MAPK antibodies),
345 3% milk/TBST (for anti-Vinculin, Lamin A/C, Akt, phospho-Akt, TSC2, and phospho-TSC2 antibodies)
346 or 5% Milk/TBST (for anti-GAPDH antibody). Membranes were visualised after secondary antibody
347 incubation (Cell Signaling Technologies 7074 and 7076) and washing with TBST using ECL substrate
348 (Thermo Fisher Scientific 12994780). Membranes were imaged in a Gbox gel/blot imaging system
349 (Syngene) and densitometry analysis was performed using ImageJ (25).

350 **TFEB-GFP microscopy**

351 HEK293 M5R-DREADD cells were transfected overnight using Fugene® HD (Promega E2311) with
352 TFEB-GFP (MRC PPU Reagents and Services DU67822). Transfected cells were re-seeded onto 8 well
353 chamber slides (Thistle Scientific IB-80826) and allowed to recover overnight. Wells were washed
354 with PBS and starved of FBS for 2 hours except for AA starvation control wells which were only
355 starved of AA for a total of 45 minutes before imaging. Cells were stained with 2 µg/ml Hoechst
356 33342 (Thermo Fisher Scientific 62249) and stimulated with 1 µM CNO for 32 minutes before
357 imaging. Live cell images were acquired on an Ultraview VoX spinning disk confocal microscope
358 (PerkinElmer) with a 40x objective. 6 full fields of view for each condition were captured per
359 experiment, and the percentage of the total TFEB-GFP signal that was nuclear was then measured.
360 Images were analysed with ImageJ, defining GFP signals overlapping with Hoechst signals as nuclear
361 TFEB-GFP.

362 **Lysosome microscopy**

363 Cells were seeded overnight onto 8 well chamber slides and allowed to recover overnight. Cells were
364 then washed with PBS and starved of FBS for 2 hours followed by 2 hours of GPCR stimulation (see
365 above). 20 nM LysoTracker™ Red DND-99 (Thermo Fisher Scientific L7528) and 2 ug ml^{-1} Hoechst
366 33342 were added to the wells for 30 minutes before imaging. Live images were acquired on an
367 Ultraview VoX spinning disk confocal microscope (PerkinElmer) with a 63x objective. 6 full fields of
368 view for each condition were captured per experiment, and the numbers of lysosomes per cell were
369 measured. Images were analysed using the find maxima function in ImageJ.

370 **Alamar Blue assay**

371 Cells were seeded overnight in 96 well plates before being washed with PBS and treated with DMEM
372 +/- FBS and +/- GPCR agonist (see above) for 18 hours. Media was then replaced with DMEM + 10%
373 Alamar blue solution (Bio-Rad BUF012A) for 3 hours before absorbance at 570 nm and 600 nm was
374 measured on a Clariostar plus plate reader (BMG Labtech). Analysis was performed as per
375 manufacturer's recommendations.

376 **Statistical analysis**

377 All statistical analyses and graphs were produced in GraphPad Prism. Technical replicates (n) were
378 averaged for each biological replicates (N). Control and experimental condition's biological repeats
379 were compared using unpaired student's t tests. P-values are reported on graphs.

Acknowledgments

We thank Fiona Murray (University of Aberdeen) for helpful suggestions; Colin Ferguson and the Microscopy and Histology Core Facility members Lucinda Wight and Debbie Wilkinson (University of Aberdeen) for technical support. This work was funded by BBSRC (BB/V016334/1 and BB/X018229/1 to RH), British Heart Foundation (PG/19/30/34327 to DT), Novo Nordisk Foundation (NNF23SA0084103 and NNF24OC0092181 to KS), and the University of Aberdeen. The authors declare no conflict of interest.

Author contributions

Conceptualization: SJA, DT, JH, and RH; Methodology: SJA, FN, WR, KT, and JH; Investigation: SJA, FN, WR, KT, and JH; Formal Analysis: SJA, FN, and JH; Validation: SJA, FN, WR, and JH; Supervision: KS, DT, JH, and RH; Funding acquisition: KS, DT, JH and RH; Visualization: SJA, JH, and RH; Writing – original draft: SJA, FN, and RH; Writing – review & editing: SJA, KS, DT, JH, and RH.

393 # References

394 1. Shimobayashi, M., and Hall, M. N. (2014) Making new contacts: The mTOR network in
395 metabolism and signalling crosstalk. *Nat Rev Mol Cell Biol*. **15**, 155–162

396 2. Liu, G. Y., and Sabatini, D. M. (2020) mTOR at the nexus of nutrition, growth, ageing and
397 disease. *Nat Rev Mol Cell Biol*. **21**, 183–203

398 3. Napolitano, G., Di Malta, C., Esposito, A., de Araujo, M. E. G., Pece, S., Bertalot, G., Matarese,
399 M., Benedetti, V., Zampelli, A., Stasyk, T., Siciliano, D., Venuta, A., Cesana, M., Vilardo, C.,
400 Nusco, E., Monfregola, J., Calcagnì, A., Di Fiore, P. P., Huber, L. A., and Ballabio, A. (2020) A
401 substrate-specific mTORC1 pathway underlies Birt–Hogg–Dubé syndrome. *Nature*. **585**, 597–
402 602

403 4. Hasegawa, J., Tokuda, E., Yao, Y., Sasaki, T., Inoki, K., and Weisman, L. S. (2022) PP2A-
404 dependent TFEB activation is blocked by PIKfyve-induced mTORC1 activity. *Mol Biol Cell*.
405 10.1091/mbc.E21-06-0309

406 5. Fernandes, S. A., Angelidaki, D.-D., Nüchel, J., Pan, J., Gollwitzer, P., Elkis, Y., Artoni, F., Wilhelm,
407 S., Kovacevic-Sarmiento, M., and Demetriades, C. (2024) Spatial and functional separation of
408 mTORC1 signalling in response to different amino acid sources. *Nat Cell Biol*. **26**, 1918–1933

409 6. Cui, Z., Napolitano, G., de Araujo, M. E. G., Esposito, A., Monfregola, J., Huber, L. A., Ballabio,
410 A., and Hurley, J. H. (2023) Structure of the lysosomal mTORC1–TFEB–Rag–Ragulator
411 megacomplex. *Nature*. **614**, 572–579

412 7. Pierce, K. L., Premont, R. T., and Lefkowitz, R. J. (2002) Seven-transmembrane receptors. *Nat*
413 *Rev Mol Cell Biol*. **3**, 639–650

414 8. Rosenbaum, D. M., Rasmussen, S. G. F., and Kobilka, B. K. (2009) The structure and function of
415 G-protein-coupled receptors. *Nature*. **459**, 356–363

416 9. Hauser, A. S., Attwood, M. M., Rask-Andersen, M., Schiöth, H. B., and Gloriam, D. E. (2017)
417 Trends in GPCR drug discovery: New agents, targets and indications. *Nat Rev Drug Discov*. **16**,
418 829–842

419 10. Milligan, G., and Kostenis, E. (2006) Heterotrimeric G-proteins: A short history. *Br J Pharmacol*.
420 10.1038/sj.bjp.0706405

421 11. Goldsmith, Z. G., and Dhanasekaran, D. N. (2007) G Protein regulation of MAPK networks.
422 *Oncogene*. **26**, 3122–3142

423 12. Scheerer, P., and Sommer, M. E. (2017) Structural mechanism of arrestin activation. *Curr Opin*
424 *Struct Biol*. **45**, 160–169

425 13. Irannejad, R., and Von Zastrow, M. (2014) GPCR signaling along the endocytic pathway. *Curr*
426 *Opin Cell Biol*. **27**, 109–116

427 14. Melick, C. H., Lama-Sherpa, T. D., Curukovic, A., and Jewell, J. L. (2022) G-Protein Coupled
428 Receptor Signaling and Mammalian Target of Rapamycin Complex 1 Regulation. *Mol*
429 *Pharmacol*. **101**, 181–190

430 15. Atwood, B. K., Lopez, J., Wager-Miller, J., Mackie, K., and Straiker, A. (2011) Expression of G
431 protein-coupled receptors and related proteins in HEK293, AtT20, BV2, and N18 cell lines as
432 revealed by microarray analysis. *BMC Genomics*. 10.1186/1471-2164-12-14

433 16. Urban, D. J., and Roth, B. L. (2015) DREADDs (designer receptors exclusively activated by
434 designer drugs): Chemogenetic tools with therapeutic utility. *Annu Rev Pharmacol Toxicol*. **55**,
435 399–417

436 17. Piecyk, M., Fauvre, J., Duret, C., Chaveroux, C., and Ferraro-Peyret, C. (2024) SUrface SEnsing
437 of Translation (SUnSET), a Method Based on Western Blot Assessing Protein Synthesis Rates in
438 vitro. *Bio Protoc*. 10.21769/BioProtoc.4933

439 18. Puertollano, R., Ferguson, S. M., Brugarolas, J., and Ballabio, A. (2018) The complex
440 relationship between TFEB transcription factor phosphorylation and subcellular localization .
441 *EMBO J*. 10.15252/embj.201798804

442 19. Mccluskey, A., Daniel, J. A., Hadzic, G., Chau, N., Clayton, E. L., Mariana, A., Whiting, A.,
443 Gorgani, N. N., Lloyd, J., Quan, A., Moshkanbaryans, L., Krishnan, S., Perera, S., Chircop, M.,
444 von Kleist, L., Mcgeachie, A. B., Howes, M. T., Parton, R. G., Campbell, M., Sakoff, J. A., Wang,
445 X., Sun, J. Y., Robertson, M. J., Deane, F. M., Nguyen, T. H., Meunier, F. A., Cousin, M. A., and
446 Robinson, P. J. (2013) Building a better dynasore: The dyngo compounds potently inhibit
447 dynamin and endocytosis. *Traffic*. **14**, 1272–1289

448 20. Klauer, M. J., Hall, K. L., Jagla, C. A. D., and Tsvetanova, N. G. (2025) Extensive location bias of
449 the GPCR-dependent translatome via site-selective activation of mTOR. *Proceedings of the*
450 *National Academy of Sciences*. 10.1073/pnas.2414738122

451 21. Thompson, D., McArthur, S., Hislop, J. N., Flower, R. J., and Perretti, M. (2014) Identification of
452 a novel recycling sequence in the C-tail of FPR2/ALX receptor: Association with cell protection
453 from apoptosis. *Journal of Biological Chemistry*. **289**, 36166–36178

454 22. Ma, L., Chen, Z., Erdjument-Bromage, H., Tempst, P., and Pandolfi, P. P. (2005) Phosphorylation
455 and functional inactivation of TSC2 by Erk: Implications for tuberous sclerosis and cancer
456 pathogenesis. *Cell*. **121**, 179–193

457 23. Hatakeyama, R., Péli-Gulli, M. P., Hu, Z., Jaquenoud, M., Garcia Osuna, G. M., Sardu, A.,
458 Dengjel, J., and De Virgilio, C. (2019) Spatially Distinct Pools of TORC1 Balance Protein
459 Homeostasis. *Mol Cell*. **73**, 325-338.e8

460 24. Armbruster, B. N., Li, X., Pausch, M. H., Herlitze, S., and Roth, B. L. (2007) Evolving the lock to
461 fit the key to create a family of G protein-coupled receptors potently activated by an inert
462 ligand. **104**, 5163–5168

463 25. Schindelin, J., Arganda-Carreras, I., Frise, E., Kaynig, V., Longair, M., Pietzsch, T., Preibisch, S.,
464 Rueden, C., Saalfeld, S., Schmid, B., Tinevez, J. Y., White, D. J., Hartenstein, V., Eliceiri, K.,
465 Tomancak, P., and Cardona, A. (2012) Fiji: An open-source platform for biological-image
466 analysis. *Nat Methods*. **9**, 676–682

467

468

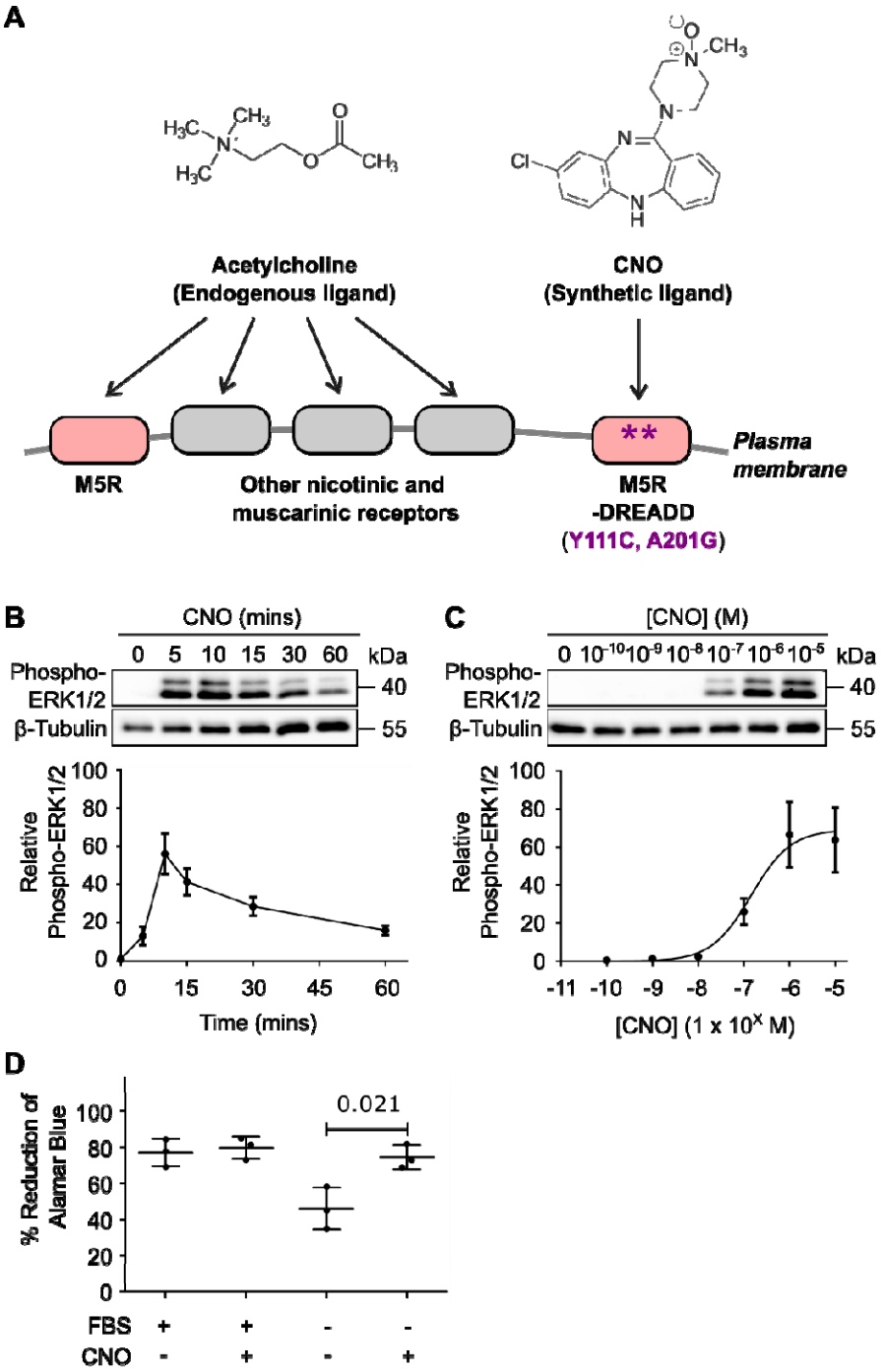
A
Acetylcholine
(Endogenous ligand)
CNO
(Synthetic ligand)
M5R
Other nicotinic and
muscarinic receptors
M5R
-DREADD
(Y111C, A201G)
Plasma
membrane
B
CNO (mins)
0 5 10 15 30 60 kDa
Phospho-
ERK1/2
β-Tubulin
40
55
Relative
Phospho-ERK1/2
Time (mins)
C
[CNO] (M)
0 10-10 10-9 10-8 10-7 10-6 10-5 kDa
Phospho-
ERK1/2
β-Tubulin
40
55
Relative
Phospho-ERK1/2
[CNO] (1 x 10X M)
D
% Reduction of
Alamar Blue
0.021
FBS + + - -
CNO - + - +

Figure 1

Figure 1. Construction and validation of the M5R-DREADD cell line.

(A) Experimental setting for M5R-specific stimulation. M5R was converted into M5R-DREADD by introducing the indicated point mutations. In cells stably expressing M5R-DREADD, the synthetic ligand CNO selectively stimulates M5R-DREADD, unlike the endogenous M5R ligand acetylcholine which binds to nicotinic and muscarinic receptor subtypes. **(B)** HEK293 cells expressing M5R-DREADD were serum starved for 2 hours prior to stimulation with 1 µM CNO for the indicated time. Cells were lysed and analysed by SDS-PAGE and western blotting. Quantitative analysis of N = 3 experiments is shown at the bottom. **(C)** HEK293 cells expressing M5R-DREADD were serum starved for 2 hours prior to stimulation with the indicated concentration of CNO for 7 minutes. Cells were lysed and analysed by SDS-PAGE and western blotting. Quantitative analysis of N = 3 experiments is shown at the bottom. **(D)** Metabolic activity of HEK293 cells expressing M5R-DREADD was measured by the reduction of Alamar Blue after overnight stimulation with 1 µM of CNO with or without serum starvation.

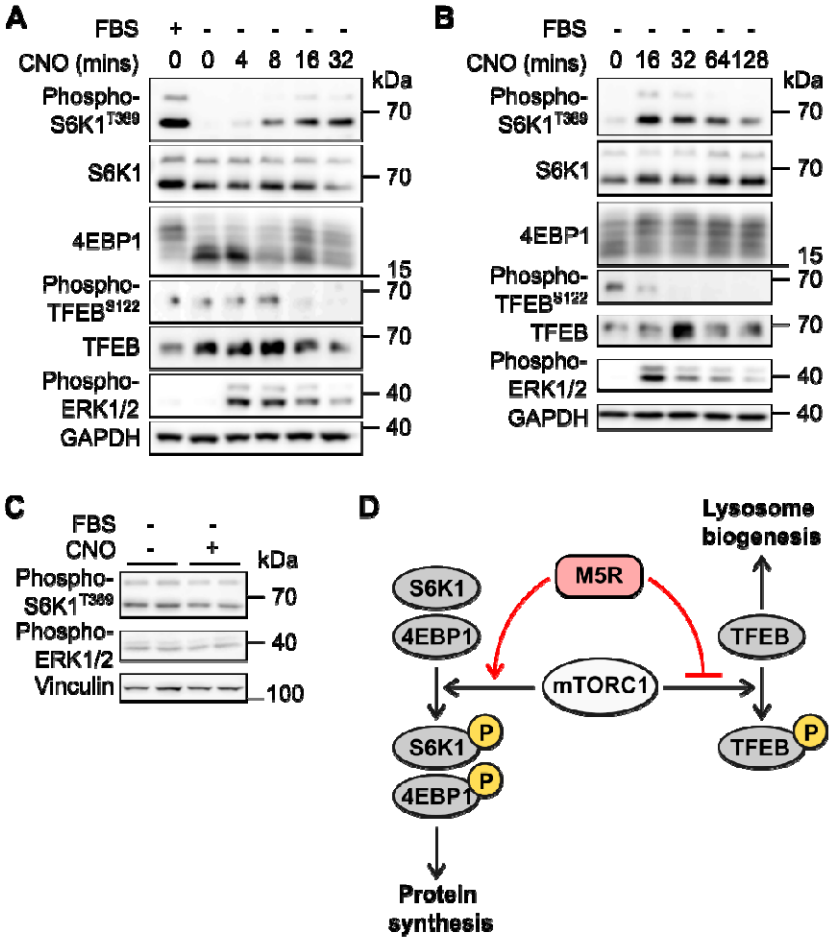

Figure 2

485

486

487 **Figure 2. Substrate-specific regulation of mTORC1 by M5R.**

488 **(A)** HEK293 cells expressing M5R-DREADD were starved of FBS or given fresh FBS-containing media
489 for 2 hours before being stimulated with 1 µM CNO for up to 32 minutes. Cells were lysed and
490 analysed by SDS-PAGE and western blotting. **(B)** HEK293 cells expressing M5R-DREADD were starved
491 of FBS or given fresh FBS-containing media for 2 hours before being stimulated with 1 µM CNO for up
492 to 128 minutes. Cells were lysed and analysed by SDS-PAGE and western blotting. **(C)** Wild-type
493 HEK293 cells were starved of FBS or given fresh FBS-containing media for 2 hours before being
494 stimulated with 1 µM CNO for 32 minutes. Cells were lysed and analysed by SDS-PAGE and western
495 blotting. **(D)** Schematic showing the proposed dualistic regulation of mTORC1 substrates by M5R.
496 S6K1/4EBP1 phosphorylation is promoted and TFEB phosphorylation is suppressed by M5R, resulting
497 in simultaneous activation of all three substrates.

498

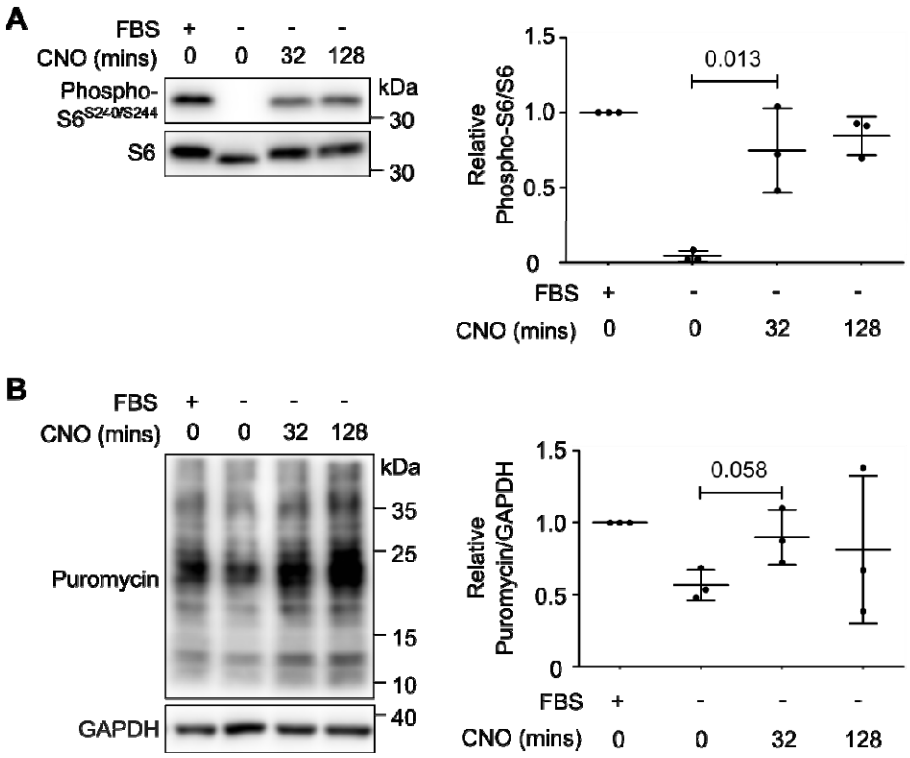
A
FBS + - - -
CNO (mins) 0 0 32 128
Phospho-S6S240/S244
S6
kDa
30
30
Relative Phospho-S6/S6
1.5
1.0
0.5
0
0.013
FBS + - - -
CNO (mins) 0 0 32 128
B
FBS + - - -
CNO (mins) 0 0 32 128
Puromycin
GAPDH
kDa
35
25
15
10
40
Relative Puromycin/GAPDH
1.5
1.0
0.5
0
0.058
FBS + - - -
CNO (mins) 0 0 32 128

Figure 3

501 **Figure 3. M5R stimulates protein synthesis.**

502 **(A)** HEK293 cells expressing M5R-DREADD were starved of FBS or given fresh FBS-containing media
503 for 2 hours before being stimulated with 1 µM CNO for the indicated times. Cells were lysed and
504 analysed by SDS-PAGE and western blotting. Quantitative analysis of N = 3 experiments is shown on
505 the right. **(B)** HEK293 cells expressing M5R-DREADD were starved of FBS or given fresh FBS-
506 containing media for 2 hours before being stimulated with 1 µM CNO for the indicated times.
507 Puromycin was added at 5 µg/ml to each condition for 15 minutes before lysis and analysis by SDS-
508 PAGE and western blotting. Quantitative analysis of N = 3 experiments is shown on the right.

509

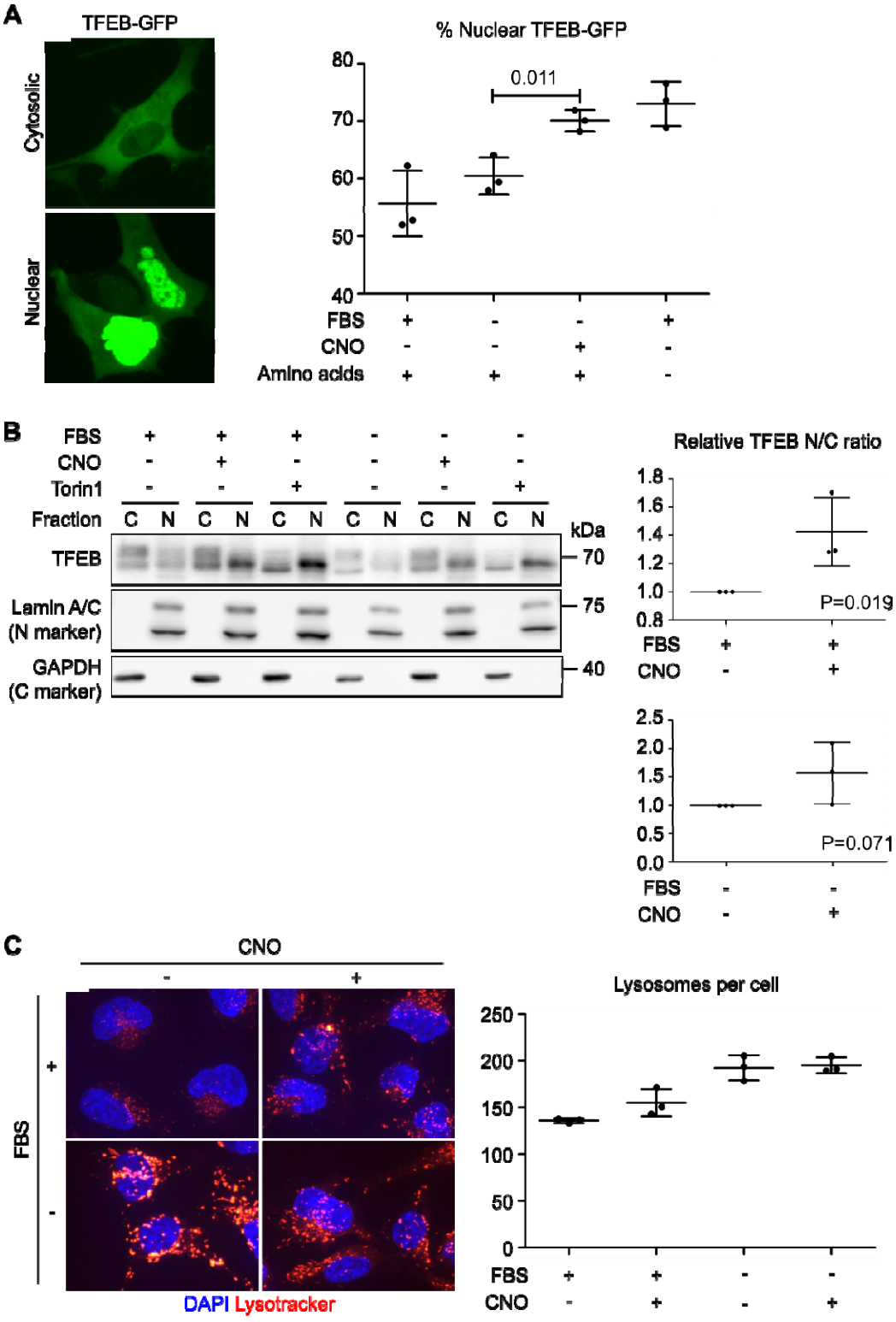
A
TFEB-GFP
Cytosolic
Nuclear
% Nuclear TFEB-GFP
0.011
80
70
60
50
40
FBS + - - +
CNO - - + -
Amino acids + + + -
B
FBS + + + - - -
CNO - + - - + -
Torin1 - - + - - +
Fraction C N C N C N C N C N C N
kDa
TFEB
70
Lamin A/C
(N marker)
75
GAPDH
(C marker)
40
Relative TFEB N/C ratio
1.8
1.6
1.4
1.2
1.0
0.8
P=0.019
FBS + +
CNO - +
2.5
2.0
1.5
1.0
0.5
0.0
P=0.071
FBS - -
CNO - +
C
CNO
-
+
FBS
+
-
DAPI Lysotracker
Lysosomes per cell
250
200
150
100
50
0
FBS + + - -
CNO - + - +

Figure 4

512 **Figure 4. M5R does not inhibit lysosome biogenesis.**

513 **(A)** HEK293 cells expressing M5R-DREADD were transfected with a TFEB-GFP expressing plasmid.
514 Transfected cells were subjected to live imaging of GFP and nuclei (using Hoechst 33342 staining).
515 Left: representative images of cells with mostly cytosolic or mostly nuclear TFEB-GFP. Quantitative
516 analysis of N = 3 experiments is shown on the right. Scale bar: 10 µm. **(B)** HEK293 cells expressing
517 M5R-DREADD were starved of FBS or given fresh FBS-containing media for 2 hours before being
518 treated with 1 µM CNO or 100 nM Torin1 for 32 minutes. After cellular fractionation, cytoplasmic (C)
519 and nuclear (N) fractions were analysed by SDS-PAGE and western blotting. Quantitative analysis of N
520 = 3 experiments is shown on the right. (**C**) HEK293 cells expressing M5R-DREADD were starved of FBS
521 for 2 hours before stimulation with 1 µM CNO for 2 hours (where indicated). Lysosomes and nuclei
522 were stained with 20 nM LysoTracker™ Red DND-99 and 2 µg/ml Hoechst 33342, respectively, before
523 live imaging. Quantitative analysis of N = 3 experiments is shown on the right. Scale bar: 10 µm.

524

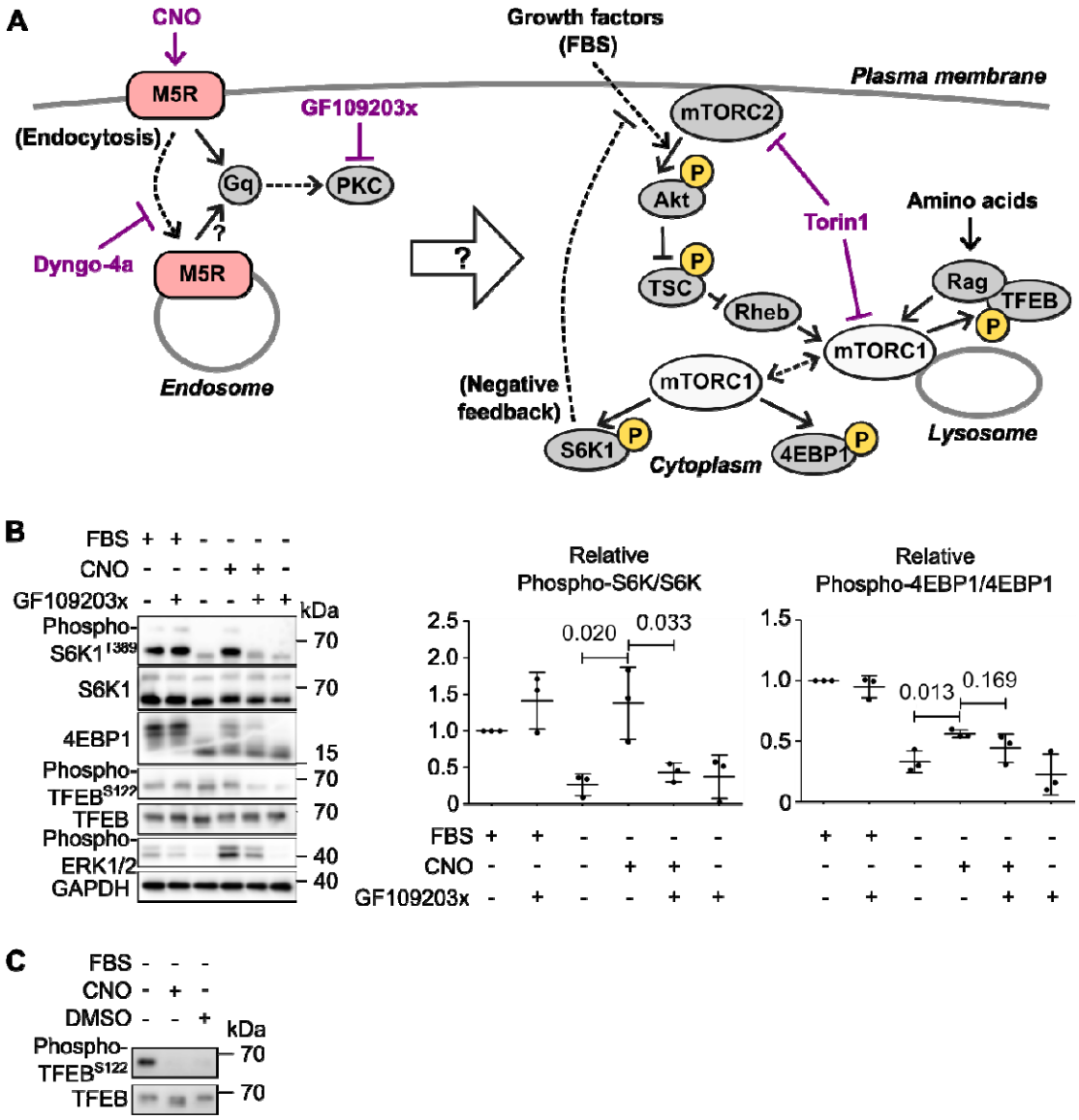
A
CNO
M5R
(Endocytosis)
Gq
PKC
GF109203x
Dyngo-4a
M5R
Endosome
Growth factors
(FBS)
Plasma membrane
mTORC2
Akt
TSC
Rheb
Torin1
Amino acids
Rag
TFEB
mTORC1
Lysosome
(Negative
feedback)
mTORC1
S6K1
4EBP1
Cytoplasm
B
FBS
CNO
GF109203x
kDa
Phospho-S6K1
S6K1
4EBP1
Phospho-TFEB
TFEB
Phospho-ERK1/2
GAPDH
Relative
Phospho-S6K/S6K
0.020
0.033
Relative
Phospho-4EBP1/4EBP1
0.013
0.169
C
FBS
CNO
DMSO
kDa
Phospho-TFEB
TFEB

525

Figure 5

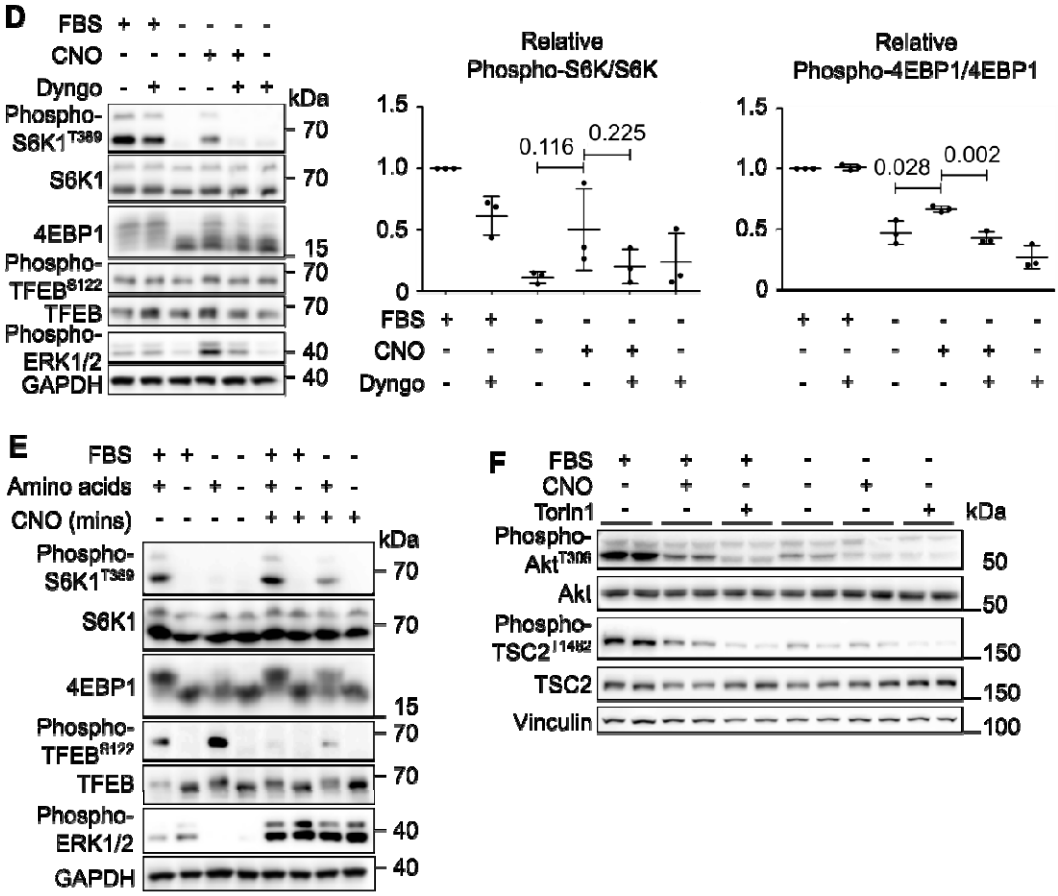

Figure 5 continued

528 **Figure 5. Mechanistic insights into the M5R-mTORC1 signaling.**

529 **(A)** Schematic outlying possible signaling modes of M5R to mTORC1. The points of action of CNO,
530 GF109203x, Dyngo®-4a, and Torin1 are shown in purple. **(B)** HEK293 cells expressing M5R-DREADD
531 were starved of FBS or given fresh FBS-containing media for 2 hours before being stimulated with 1
532 µM CNO for 32 minutes. PKC was inhibited using 5 µM GF109203x for 1.5 hours before CNO
533 treatment. Cells were lysed and analysed by SDS-PAGE and western blotting. Quantitative analysis of
534 N = 3 experiments is shown on the right. **(C)** HEK293 cells expressing M5R-DREADD were starved of
535 FBS or given fresh FBS-containing media for 2 hours before being treated with 1 µM CNO for 32
536 minutes or DMSO at 1:2000 for 1.5 hours. Cells were lysed and analysed by SDS-PAGE and western
537 blotting. **(D)** HEK293 cells expressing M5R-DREADD were starved of FBS or given fresh FBS-containing
538 media for 2 hours before being stimulated with 1 µM CNO for 32 minutes. The Dynamin inhibitor
539 Dyngo®-4a (to prevent endocytosis) was added at 10 µM for 30 minutes before CNO treatment. Cells
540 were lysed and analysed by SDS-PAGE and western blotting. Quantitative analysis of N = 3
541 experiments is shown on the right. **(E)** HEK293 cells expressing M5R-DREADD were starved of FBS,
542 amino acids, or both, or given fresh FBS-containing media for 2 hours before being stimulated with 1
543 µM CNO for 32 minutes. Cells were lysed and analysed by SDS-PAGE and western blotting. **(F)**
544 HEK293 cells expressing M5R-DREADD were starved of FBS or given fresh FBS-containing media for 2
545 hours before being treated with 1 µM CNO or 100 nM Torin1 for 32 minutes. Cells were lysed and
546 analysed by SDS-PAGE and western blotting.

547

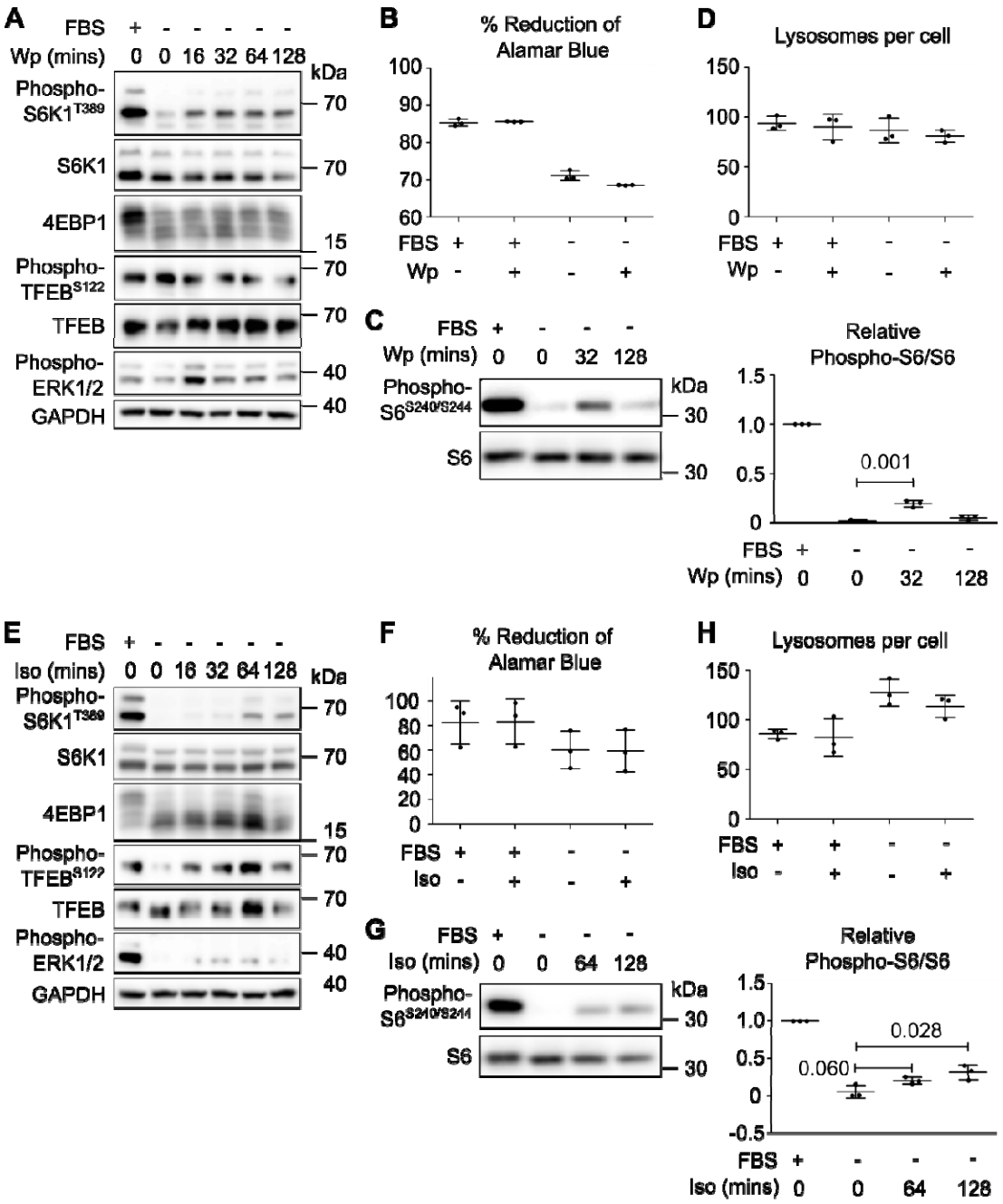

Figure 6

548

549

550 **Figure 6. Differential response of mTORC1 substrates to other GPCRs.**

551 **(A)** HEK293 cells expressing FPR2 were starved of FBS or given fresh FBS-containing media for 2 hours
552 before being stimulated with 1 µM WKYMVm peptide (Wp) for up to 128 minutes. Cells were lysed
553 and analysed by SDS-PAGE and western blotting. **(B)** Metabolic activity of HEK293 cells expressing
554 FPR2 was measured by the reduction of Alamar Blue after overnight stimulation with 1 µM
555 WKYMVm peptide with or without serum starvation. **(C)** HEK293 cells expressing FPR2 were starved
556 of FBS or given fresh FBS-containing media for 2 hours before being stimulated with 1 µM WKYMVm
557 peptide for the indicated times. Cells were lysed and analysed by SDS-PAGE and western blotting.
558 Quantitative analysis of N = 3 experiments is shown on the right. **(D)** HEK293 cells expressing FPR2
559 were starved of FBS for 2 hours before stimulation with 1 µM WKYMVm peptide for 2 hours (where
560 indicated). Lysosomes and nuclei were stained with 20 nM LysoTracker™ Red DND-99 and Hoechst
561 33342 before live imaging. The result of a quantitative analysis of N = 3 experiments is shown. **(E)**
562 Wild-type HEK293 cells were starved of FBS or given fresh FBS-containing media for 2 hours before
563 being stimulated with 1 µM isoprenaline (Iso) for up to 128 minutes. Cells were lysed and analysed
564 by SDS-PAGE and western blotting. **(F)** Metabolic activity of wild-type HEK293 cells was measured by
565 the reduction of Alamar Blue after overnight stimulation with 1 µM isoprenaline with or without
566 serum starvation. **(G)** Wild-type HEK293 cells were starved of FBS or given fresh FBS-containing
567 media for 2 hours before being stimulated with 1 µM isoprenaline for the indicated times. Cells were
568 lysed and analysed by SDS-PAGE and western blotting. Quantitative analysis of N = 3 experiments is
569 shown on the right. **(H)** Wild-type HEK293 cells were starved of FBS for 2 hours before stimulation
570 with 1 µM isoprenaline for 2 hours (where indicated). Lysosomes and nuclei were stained with 20 nM
571 LysoTracker™ Red DND-99 and Hoechst 33342 before live imaging. The result of a quantitative
572 analysis of N = 3 experiments is shown.